

---

# Towards Open Set 3D Learning: A Benchmark on Object Point Clouds

---

**Antonio Alliegro, Francesco Cappio Borlino, Tatiana Tommasi**

Department of Control and Computer Engineering, Politecnico di Torino, Italy

Italian Institute of Technology, Italy

{antonio.alliegro, francesco.cappio, tatiana.tommasi}@polito.it

## Abstract

In the last years, there has been significant progress in the field of 3D learning on classification, detection and segmentation problems. The vast majority of the existing studies focus on canonical closed-set conditions, neglecting the intrinsic open nature of the real-world. This limits the abilities of autonomous systems involved in safety-critical applications that require managing novel and unknown signals. In this context exploiting 3D data can be a valuable asset since it conveys rich information about the geometry of sensed objects and scenes. This paper provides the first broad study on Open Set 3D learning. We introduce a novel testbed with settings of increasing difficulty in terms of category semantic shift and cover both in-domain (synthetic-to-synthetic) and cross-domain (synthetic-to-real) scenarios. Moreover, we investigate the related out-of-distribution and Open Set 2D literature to understand if and how their most recent approaches are effective on 3D data. Our extensive benchmark positions several algorithms in the same coherent picture, revealing their strengths and limitations. The results of our analysis may serve as a reliable foothold for future tailored Open Set 3D models.

## 1 Introduction

Most existing machine learning models rely on the assumption that train and test data are drawn *i.i.d.* from the same distribution. While reasonable for lab experiments, this assumption frequently fails to hold when models are deployed in the open world, where a variety of distributional shifts with respect to the training data can emerge. For example, new object categories may induce a semantic shift, or data from new domains may give rise to a covariate shift [55, 56, 37]. Such cases can occur separately or jointly, and the test samples that differ from what was observed during training are generally indicated as out-of-distribution (OOD) data. These data may become extremely dangerous for autonomous agents as testified by the numerous accidents involving self-driving cars that misbehaved when encountering anomalous objects in the streets<sup>1</sup>. To avoid similar risks it is of paramount importance to build robust models capable of maintaining their discrimination ability over the closed set of known classes while rejecting unknown categories. Solving this task is challenging for existing deep models: their exceptional closed set performance hides miscalibration [17] and over-confidence issues [34]. In other words, their output score cannot be regarded as a reliable measure of prediction correctness. This drawback has been largely discussed in the 2D visual learning literature [43, 7, 59, 47] as its solution would enable the use of powerful deep models for many real-world tasks. In this context, and particularly for many safety-critical applications such as self-driving cars, 3D sensing is a valuable asset, providing detailed information about the geometry of sensed objects that 2D images cannot capture. However 3D literature in this field is still in its

---

<sup>1</sup><https://edition.cnn.com/2021/08/27/cars/toyota-self-driving-vehicle-paralympics-accident/index.html>  
<https://www.foxnews.com/auto/tesla-smashes-overtuned-truck-autopilot>


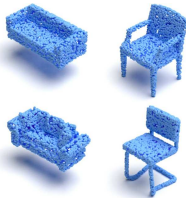
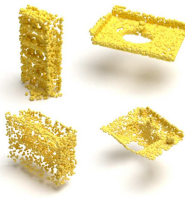

|                       | training synth.   | test synth.   | test real  |   |
|-----------------------|---|---|--|---|
| Data                  |  |  |  |  |
| OOD                   | known<br>in-distribution<br>bookshelf, sink                                       | unknown   | unknown  | unknown   |
| semantic<br>nov. det. |   | unknown   | known  | unknown   |
| Open Set              |   | unknown   | bookshelf, sink  | unknown   |

Figure 1: Schematic illustration of the OOD, semantic novelty detection and Open Set tasks on 3D data. The blue instances are synthetic point clouds from ModelNet40 [51]. The yellow instances are from the real-world ScanObjectNN [46] dataset.

infancy, with only a small number of works which have just started to scratch the surface of the problem by focusing on particular sub-settings [32, 3]. With this work, we draw the community’s attention to Open Set 3D learning, which entails developing models designed to process 3D point clouds that can recognize test samples from a set of known categories while avoiding prediction for samples from unknown classes. Our contributions are: 1) we propose the first large-scale testbed for Open Set 3D learning, presenting several settings with increasing levels of difficulty; 2) we consider two main experimental tracks: a *Synthetic Benchmark* and a *Synthetic to Real Benchmark*. The former is designed to evaluate how existing methods deal with semantic novelty, whereas the latter includes a further domain shift on the data to simulate real-world deployment conditions. 3) we build a coherent picture by putting together the existing literature from OOD detection and Open Set recognition in 2D and 3D; 4) we analyze the performance of these methods to discover which is the state-of-the-art for Open Set 3D learning. We highlight their advantages and limitations, showing that a simple representation learning approach may outperform more sophisticated methods. Our code and data are available at [https://github.com/antoalli/3D\\_OS](https://github.com/antoalli/3D_OS).

## 2 Related Work

We provide an overview of existing literature on *OOD detection* and *Open Set learning*. The difference between these two tasks is often neglected, but it is important to point it out (see Fig. 1). In OOD detection it is sufficient to identify, and reject as unknown, samples with any distribution shift with respect to the training data. In the particular case of *semantic novelty detection*, the concept of novelty is limited to the categories not seen during training, regardless of the specific domain appearance of the observed samples. Besides separating data of known classes from those of unknown classes, Open Set recognition requires performing a class prediction over the known categories.

**Discriminative Methods.** By training a model with multi-class supervision we expect to get low uncertainty on in-distribution (ID) data and high uncertainty for OOD samples. Thus, a baseline approach may consist in using the maximum softmax probability (MSP) as a *normality score* to separate known and unknown instances [19]. However, deep models suffer from over-confidence [34] and their prediction outputs need some re-calibration to be considered as uncertainty scoring functions. ODIN [28] exploited temperature scaling and input pre-processing to better separate ID from OOD samples. In [29] the authors showed how to derive Energy scores from the prediction output, demonstrating that they are better aligned with the probability density of the inputs and are less prone to over-confidence. Instead of considering the output, GradNorm [22] focused on the network’s gradients showing that their norm carries distinctive signatures to amplify the ID/OOD separability. ReAct [43] proposed to further increase this separability by rectifying the internal network activations. Finally, a very recent work has discussed how the normalized softmax probabilities can be replaced by the maximum logit scores (MLS), resulting in an approach competitive with other more complex strategies [47]. We highlight that all the methods of this discriminative family are applied post-hoc on the closed set classifier, meaning that the original training procedure and objective are not modified. Thus, the models maintain their ability to distinguish among the known classes and are suitable for Open Set recognition.

**Density and Reconstruction Based Methods.** Density-based methods are trained to model the distribution of known data. Input samples are then identified as unknown if lying in low-likelihood regions. Several works have exploited generative models for OOD detection with novelty metrics that range from basic sample reconstruction [1, 10] to more complex likelihood ratio and regret [36, 53]. Still, generative models can be difficult to train, and their performance is frequently lower than that of discriminative ones. Recently a hybrid approach proposed to combine discriminative and probabilistic flow-based learning with promising results [59].

**Outlier Exposure.** Another line of OOD approaches exploits *outlier* data available at training time. They are used to regularize the model by applying conditions on the prediction entropy [20, 58] or running outlier mining, re-sampling and filtering [9, 27, 55].

**OOD Data Generation.** In many practical cases, it is not possible to access outlier samples at training time. Thus, unknown sample synthesis is used to prepare the model for the deployment conditions [33, 14, 7, 60]. Some recent OOD approaches have also combined real outlier mining and fake outlier generation [24].

**Representation and Distance Based Methods.** Enhancing data representation may help to better characterize known data and consequently ease the identification of unknown samples. In a reliable embedding space, OOD samples should be far away from ID classes so that the distance from stored exemplars or prototypes can be used as a scoring function. Existing approaches focus on two aspects: how to learn a good representation and how to measure distances. Self-supervised, contrastive and prototypes learning methods are of the first kind and generally rely on cosine similarity [45, 8, 41]. Other solutions build on discriminative models, but instead of considering the prediction output, they focus on the learned features and evaluate samples distances by using different metrics like  $L^2$  norm, layer-wise Mahalanobis, or similarity metrics based on Gram matrices [21, 26, 39].

All the references mentioned above come from the 2D literature. Up to our knowledge 3D OOD detection and Open Set problems have been studied only by a handful of works. A VAE approach for reconstruction-based 3D OOD detection is provided in [32], together with an analysis on seven classes of the ShapeNet dataset [6], each used in turn as unknown. The study considers different VAE normality scores but does not compare with other baselines. In [3] the authors distilled knowledge from a large teacher network while also adding data produced by mixing training samples to define an unknown class. The authors focus on building a lightweight model and do not include comparisons with other Open Set methods. Moreover the classes in the used known/unknown datasets (ModelNet10/40 [51]) significantly differ in pose and headings which makes their separation trivial [25]. Two other works refer to Open Set 3D detection and segmentation, but their objective is mainly clustering to aggregate points into object instances [5, 50].

### 3 Benchmark Description

#### 3.1 Preliminaries

**Problem formulation.** We consider the labeled set  $\mathcal{S} = \{\mathbf{x}^s, y^s\}_{s=1}^N$  drawn from the training distribution  $p_{\mathcal{S}}$ , and we indicate as *known* all the classes  $y^s \in \mathcal{Y}^s$  covered by this set. A model trained on  $\mathcal{S}$  is later evaluated on the test set  $\mathcal{T} = \{\mathbf{x}^t\}_{t=1}^M$  drawn from the distribution  $p_{\mathcal{T}}$ . The two distributions may either differ only in semantic content, or present both a domain and a category shift. For the test data labels  $y^t \in \mathcal{Y}^t$  it holds  $\mathcal{Y}^s \neq \mathcal{Y}^t$ . More specifically, we consider a partial overlap between the two sets  $\mathcal{Y}^s \subset \mathcal{Y}^t$  and the test classes which do not appear in the *known* class set  $\mathcal{Y}^s$  are therefore *unknown*. A reliable semantic novelty detection model trained on  $\mathcal{S}$  should output for each test sample  $\mathbf{x}^t$  a normality score representing its probability of belonging to any of the known classes in  $\mathcal{Y}^s$ . An Open Set model must also provide an output probability distribution over each of the classes in  $\mathcal{Y}^s$ . In both cases, the models should generalize over the possible domain shift and focus only on the semantic content of the data.

**Performance Metrics.** We evaluate the ability to detect unknown samples by exploiting two metrics: **AUROC** and **FPR95**. The former is the Area Under the Receiver Operating Characteristic curve (the higher the better), obtained by varying the normality decision threshold. FPR95 (the lower the better) corresponds to the false positive rate of OOD examples when choosing a normality threshold for which the true positive rate of ID examples is 95%. For Open Set methods we also evaluate their ability to correctly classify known data by computing their classification accuracy (**ACC**).



Figure 2: Object categories in each of the sets of the Synthetic Benchmark. **SN1**: mug, lamp, bed, washer, loudspeaker, telephone, dishwasher, camera, birdhouse, jar, bowl, bookshelf, stove, bench, display, keyboard, clock, piano. **SN2**: earphone, knife, chair, pillow, table, laptop, mailbox, basket, file cabinet, sofa, printer, flowerpot, microphone, tower, bag, trash bin. **SN3**: can, microwave, skateboard, faucet, train, guitar, pistol, helmet, watercraft, airplane, bottle, cap, rocket, rifle, remote, car, bus, motorbike.



Figure 3: Object categories in each of the sets of the Synthetic to Real Benchmark. **SR1**: chair, shelf, door, sink, sofa. **SR2**: bed, toilet, desk, table, display. **SR3**: bag, bin, box, pillow, cabinet.

**Datasets.** We build our 3D Open Set benchmark on top of three well-known 3D object datasets: ShapeNetCore [6], ModelNet40 [51] and ScanObjectNN [46].

*ShapeNetCore* contains 51,127 meshes from synthetic instances of 55 common object categories. We adopt ShapeNetCore v2 and use the official training (70%), validation (10%) and test (20%) splits. All objects are consistently aligned in pose. The point clouds are obtained by uniformly sampling points from the mesh surface and they are normalized to fit within a unit cube centered at the origin. In our analysis we merge telephone and cellphone categories obtaining a total of 54 classes.

*ModelNet40* [51] contains 12,311 3D CAD models from 40 man-made object categories. We use the official dataset split, consisting of 9,843 train and 2,468 test shapes according to [35]. We obtain a point cloud from each CAD model by uniformly sampling points from the faces of the synthetic mesh. Each point cloud is then centered in the origin and scaled to fit within a unit cube.

*ScanObjectNN* [46] contains 2,902 3D scans of real-world objects from 15 categories. Specifically, we consider the original OBJ\_BG split in which the scans are affected by acquisition artifacts such as vertex noise, non-uniform density, missing parts, and occlusions. Moreover, the point clouds include background, which is absent in the synthetic models from ModelNet and ShapeNet datasets.

### 3.2 Benchmark Tracks

Our testbed includes two main Open Set tracks: the *Synthetic Benchmark* presents a semantic shift between the training and the test sets, while the more challenging *Synthetic to Real Benchmark* covers both semantic and domain shift with train and test samples that are respectively drawn from synthetic data (Modelnet40) and real-world data (ScanObjectNN).

**Synthetic Benchmark.** We employ ShapeNetCore [6] dataset and we split it into three not overlapping (*i.e.* semantically different) category sets of 18 categories each. We name them SN1, SN2 and SN3 (see Fig. 2 for the list of categories belonging to each set). We obtain three scenarios of increasing difficulty by simply selecting each of the SN-Sets in turn as *known* class set and considering the remaining two category sets as *unknown*. The models are trained on the train split of the known class set and evaluated on the test split of both known and unknown classes.

**Synthetic to Real Benchmark.** We employ synthetic point clouds from ModelNet40 [51] for training while we test on real-world point clouds from ScanObjectNN [46]. We choose to adopt ModelNet40 (instead of ShapeNetCore) because it has a better overlap with ScanObjectNN and previous works already considered the same cross-domain scenario in the context of point cloud object classification [2, 4]. We define three different category sets: SR1, SR2, and SR3 as described in Fig. 3. The first two sets are composed of matching classes from ModelNet40 and ScanObjectNN. The third set (SR3) is instead composed of ScanObjectNN classes without such a one-to-one mapping with ModelNet40. Overall we have two scenarios with either SR1 or SR2 used as *known* and the

other two considered as *unknown*. The models are trained on the known classes of ModelNet40 and evaluated on ScanObjectNN samples from both known and unknown classes.

### 3.3 Evaluated Methods

We consider several approaches from the families of methods described in Sec. 2.

**Discriminative Methods.** All these methods are built on top of a standard closed set classifier trained with cross-entropy. For our analysis we select the **MSP** [19] baseline, as well as its maximum logit score variant (**MLS**) [47]. We further consider **ODIN** [28], **Energy** [29], **GradNorm** [22] and **ReAct** [43].

**Density and Reconstruction Based Methods.** We select two methods from this group. We test a **VAE** model with reconstruction-based scoring by following one of the few existing works on 3D OOD detection [32]. This is the only unsupervised approach in our analysis: it separates known from unknown samples, but cannot provide category predictions on the known classes samples.

The second approach is based on Normalizing Flow (**NF**). We took inspiration from the 2D Open Set method OpenHybrid [59] and the anomaly detection method DifferNet [38]. Specifically, we design a multi-head architecture where the NF model consists of 8 coupling blocks [13], added on top of the feature embedding shared with a cross-entropy classifier. The training objective consists in maximizing the log-likelihood of training samples, and the predicted log-likelihood is later used to distinguish ID and OOD test samples. Differently from the VAE, this model also includes a closed set classifier which makes it suitable for the Open Set task.

**Outlier Exposure with OOD Generated Data.** In all our experimental settings the training data do not include unknown samples. To assess the performance of the OE approach presented in [20] we hallucinate OOD instances via point cloud mixup [25] (**OE+mixup**).

**Representation and Distance Based Methods.** To evaluate the effect of a carefully learned feature embedding on the identification of novel categories, we consider the 2D Open Set method **ARPL+CS** [7]. It learns reciprocal points that represent the *otherness* with respect to each known class: the distance from these points is considered proportional to the probability that a sample belongs to a certain class. Moreover, the method includes confusing samples (CS) generated in an adversarial manner to represent samples of unseen classes which are equidistant from all the reciprocal points. We also test the embedding of a cosine classifier (**Cosine proto**) as done in [16], this method learns class prototypes by maximizing the cosine similarity between each training sample and the prototype of its class. At inference time the highest cosine similarity with a known class prototype is used as a normality score. As a further reference, we consider the embedding space learned by optimizing the standard supervised cross-entropy and the supervised contrastive [23] losses. In the first case, we rely on the euclidean distance between the features of the test sample and the nearest training sample (**CE** ( $L^2$ )), while in the second (**SupCon**) we use the cosine distance which better reflects the contrastive training objective. In this analysis of distance-based models we also include a seemingly unconnected technique originally proposed for face recognition. The **SubArcFace** [11] approach belongs to the family of margin-based softmax methods that aim at simultaneously achieving maximal intra-class compactness and inter-class discrepancy. This objective is similar to that attained by contrastive models, but it comes without the drawbacks of complex negative sampling and large data batches. With respect to other similar strategies [12, 48], SubArcFace identifies multiple sub-centers for each known class, and a training sample only needs to be close to one of them rather than to a single class prototype. To get the normality score we follow the same procedure adopted for SupCon. We remark that the last three listed methods (CE ( $L^2$ ), SupCon, SubArcface) require training data to be available at test time because the normality score of the test sample corresponds to its distance from the nearest train sample.

### 3.4 Implementation Details.

We perform our analysis by focusing on two reliable backbones: DGCNN [49] and PointNet++ [35].

Unless otherwise specified, we use point clouds with 1024 sampled points for both training and testing. In the Synthetic Benchmark we augment training data with scale and translation transformations, for the Synthetic to Real case we add augmentations by random rotation around the up-axis. All models are trained with a batch size of 64 for 250 epochs, with exception of SubArcFace which

Table 1: Results on the Synthetic Benchmark track. Each column title indicates the chosen known class set, the other two sets serve as unknown. The difficulty of each task depends on the semantic difference between the train and test sets.

| Method          | Synthetic Benchmark - DGCNN [49] |             |             |             |             |             | Synthetic Benchmark - PointNet++ [35] |             |             |             |             |             |             |             |             |             |
|-----------------|----------------------------------|-------------|-------------|-------------|-------------|-------------|---------------------------------------|-------------|-------------|-------------|-------------|-------------|-------------|-------------|-------------|-------------|
|                 | SN1 (hard)                       |             | SN2 (med)   |             | SN3 (easy)  |             | SN1 (hard)                            |             | SN2 (med)   |             | SN3 (easy)  |             | Avg         |             |             |             |
|                 | AUROC↑                           | FPR95↓      | AUROC↑      | FPR95↓      | AUROC↑      | FPR95↓      | AUROC↑                                | FPR95↓      | AUROC↑      | FPR95↓      | AUROC↑      | FPR95↓      | AUROC↑      | FPR95↓      |             |             |
| MSP [19]        | 74.0                             | 83.9        | 88.6        | 62.4        | 92.9        | 43.2        | 85.2                                  | 63.2        | 74.3        | 82.8        | 80.0        | 78.1        | 89.7        | 52.2        | 81.3        | 71.0        |
| MLS [47]        | 75.1                             | 77.7        | 91.1        | 42.6        | 92.4        | 35.2        | 86.2                                  | 51.8        | 72.0        | 80.8        | 83.9        | 64.1        | 89.8        | 40.5        | 81.9        | 61.8        |
| ODIN [28]       | 75.4                             | 76.5        | 91.1        | 42.9        | 92.5        | 34.4        | 86.3                                  | 51.3        | 74.2        | 79.4        | 79.4        | 71.7        | 87.8        | 41.8        | 80.5        | 64.3        |
| Energy [29]     | 75.2                             | 77.0        | 91.2        | 41.6        | 92.3        | 36.4        | 86.2                                  | 51.7        | 72.1        | 81.2        | 84.0        | 64.7        | 89.8        | 39.4        | 82.0        | 61.8        |
| GradNorm [22]   | 66.2                             | 88.1        | 80.9        | 64.0        | 71.6        | 77.7        | 72.9                                  | 76.6        | 72.1        | 81.8        | 57.7        | 88.9        | 57.8        | 79.0        | 62.6        | 83.3        |
| ReAct [43]      | 76.4                             | 74.6        | 92.5        | 37.9        | 96.4        | 19.3        | 88.4                                  | 43.9        | 73.7        | 79.4        | <b>89.6</b> | 52.1        | <b>95.0</b> | <b>27.2</b> | 86.1        | 52.9        |
| VAE [32]        | 67.2                             | 76.9        | 69.5        | 83.4        | 94.3        | 32.4        | 77.0                                  | 64.2        | -           | -           | -           | -           | -           | -           | -           | -           |
| NF              | 82.0                             | 74.8        | 86.1        | 53.8        | <b>97.4</b> | <b>11.5</b> | 88.5                                  | 46.7        | 81.5        | 72.5        | 71.1        | 78.0        | 91.0        | 49.6        | 81.2        | 66.7        |
| OE+mixup [20]   | 73.7                             | 78.9        | 90.4        | 44.7        | 91.4        | 46.0        | 85.2                                  | 56.5        | 72.7        | 78.9        | 80.3        | 68.8        | 87.3        | 62.2        | 80.1        | 69.9        |
| ARPL+CS [7]     | 72.9                             | 84.2        | 90.7        | 47.1        | 89.5        | 89.5        | 84.4                                  | 73.6        | 74.8        | 80.3        | 80.7        | 72.4        | 85.4        | 50.8        | 80.3        | 67.8        |
| Cosine proto    | <b>84.3</b>                      | <b>59.1</b> | 88.8        | 39.7        | 86.4        | 48.0        | 86.5                                  | 48.9        | 80.3        | 68.3        | 88.7        | 60.8        | 91.9        | 38.0        | 86.9        | 55.7        |
| CE ( $L^2$ )    | 80.4                             | 75.5        | 90.1        | <b>40.9</b> | 96.7        | 14.4        | 89.1                                  | <b>43.6</b> | <b>83.4</b> | <b>66.8</b> | 89.5        | <b>37.7</b> | 92.9        | 28.1        | <b>88.6</b> | <b>44.2</b> |
| SupCon [23]     | 80.3                             | 75.7        | 84.6        | 73.6        | 87.9        | 44.3        | 84.3                                  | 64.5        | 80.9        | 75.5        | 83.5        | 68.2        | 85.1        | 45.1        | 83.2        | 62.9        |
| SubArcface [11] | 81.2                             | 73.4        | <b>91.9</b> | 44.0        | 94.9        | 26.5        | <b>89.3</b>                           | 48.0        | 79.0        | 81.2        | 82.9        | 60.3        | 89.1        | 32.8        | 83.7        | 58.1        |

Table 2: Relationship between closed and open set performance when training a discriminative model via the addition of Label Smoothing (LS). We show the results on the hard SN1 set.

|        | SN1 (hard) - Synthetic Benchmark - DGCNN [49] |      |      |      |              |      | SN1 (hard) - Synthetic Benchmark - PointNet++ [35] |      |      |        |      |        |              |      |                |      |
|--------|---|------|------|------|--------------|------|--|------|------|--------|------|--------|--------------|------|----------------|------|
|        | MSP   | +LS  | MLS  | +LS  | CE ( $L^2$ ) | +LS  | Closed set Acc                                     | +LS  | MSP  | MSP+LS | MLS  | MLS+LS | CE ( $L^2$ ) | +LS  | Closed set Acc | +LS  |
| AUROC↑ | 74.0  | 77.4 | 75.1 | 77.5 | 80.4         | 80.2 | 85.5   | 86.0 | 74.3 | 72.7   | 72.0 | 69.6   | 83.4         | 79.1 | 85.9           | 86.3 |
| FPR95↓ | 83.9  | 73.7 | 77.7 | 71.8 | 75.5         | 66.7 | -  | -    | 82.8 | 78.6   | 80.8 | 77.6   | 66.8         | 77.4 | -              | -    |

is trained for 500 epochs on synthetic sets (SN1, SN2, SN3). For the DGCNN experiments we use SGD optimizer with an initial learning rate of 0.1; momentum and weight decay are set respectively to 0.9 and 0.0001. With PointNet++ we employ Adam optimizer and set the initial learning rate to 0.001. Each experiment is repeated with three different seeds: the results are taken from the last epoch model and averaged across seeds. Our code is implemented in PyTorch, and the experiments run on an HPC cluster with NVIDIA V100 GPUs. See the Appendix for further details.

## 4 Synthetic Benchmark Experiments

**How do 2D methods perform on 3D Open Set tasks?** Our first set of experiments aims at analysing the performance of OOD detection and Open Set methods mainly inherited from the 2D literature on our 3D Synthetic Benchmark. We report results in Tab. 1, following the same four-group organization of Sec.3.3.

*Discriminative Methods.* We consider MSP as the main baseline, but we include also its variant MLS [47]. We can see that the latter is a strong baseline, as it is often on par or better than more complex competitors (e.g. ODIN, Energy, GradNorm). In general, all methods of this group manage to improve the MSP baseline results both in terms of AUROC and FPR95, with the only exception of GradNorm. The peculiarity of this approach is that it relies on gradients extracted at test time from the network layers to compute the normality score. We hypothesize that the substantial difference between 2D (for which the model has been originally designed) and 3D network architectures may be responsible for the observed poor performance. ReAct consistently outperforms all the other methods with both the DGCNN and PointNet++ backbones.

*Density and Reconstruction Based Methods.* VAE results are far below the MSP baseline, this could be expected since it is the only unsupervised method in the table. It should be noted that its encoder does not correspond to either DGCNN or PointNet++. It is composed of graph-convolutional and MLP layers, while the decoder is inspired by FoldingNet [57]. Still, VAE was used in one of the few existing 3D OOD detection works [32], so we decided to keep it in our analysis as a reference. The results of NF show a different trend depending on the chosen backbone: the performance is high when NF is trained on top of the semantically rich embedding extracted by DGCNN, while it underperforms on the PointNet++ whose embedding mainly captures local structures.

*Outlier Exposure with OOD Generated Data.* Comparing with the MSP baseline we observe that for both backbones the OE finetuning produces a slight improvement in terms of FPR95 while the AUROC does not show any gain.

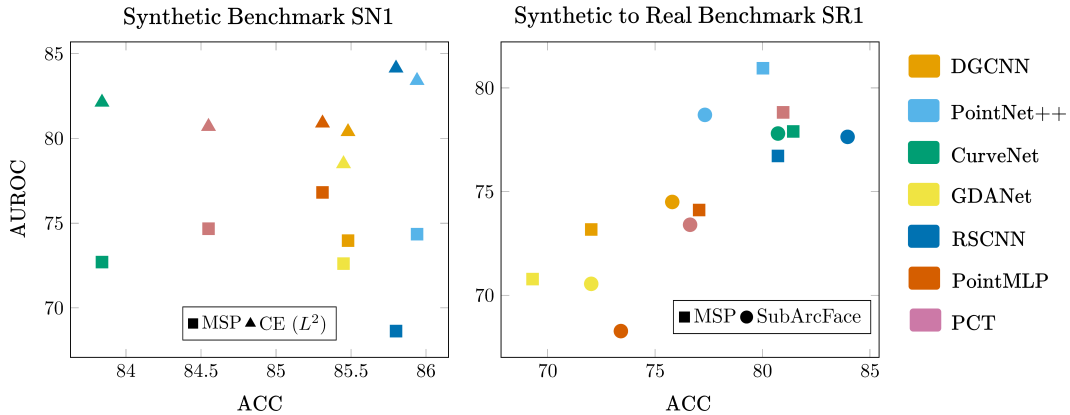


Figure 4: Correlation between open set (AUROC) and closed set (Acc) performance when changing the backbone on the Synthetic Benchmark SN1 case (left) and the Synthetic to Real Benchmark SR1 case (right).

*Representation and Distance Based Methods.* The ARPL+CS [7] approach is the current state-of-the-art 2D Open Set method, however the results indicate that it does not work as well on 3D data and it is easily outperformed by the much simpler Cosine proto. Interestingly, the very simple CE ( $L^2$ ) method built on a standard cross entropy classifier obtains promising results for both backbones and outperforms all the competing methods. The same considerations made for ARPL+CS hold for SupCon, which was successfully used in the past for OOD detection in 2D [45, 40]. Despite contrastive models have shown to be effective for 3D object classification and segmentation tasks, the learned embedding does not seem able to capture relevant cues to discriminate between known and unknown data. Part of the reason may be due to the limited variability observed in the very clean synthetic data. Better results can be obtained with SubArcFace whose objective is similar to that of contrastive models, but its formulation is much less demanding in terms of data quantity and converges more easily. From this analysis, the CE ( $L^2$ ) approach emerges as the more reliable method with top results on both backbones. In the following, we will primarily focus on it, along with MSP and MLS as baselines.

**What is the effect of improving closed-set classification on 3D Open Set?** A recent work has put under the spotlight the correlation between the closed set accuracy of discriminative models with their Open Set recognition performance on images [47]. To verify this trend on 3D data we run two sets of experiments on the most challenging SN1 case. A first analysis is done by exploiting a standard regularization technique as label smoothing (LS, [44]). Tab. 2 shows that LS provides a small closed set accuracy improvement (ACC) for both backbones, as well as some improvement on the Open Set metrics AUROC and FPR95 when using the DGCNN backbone. With PointNet++ the advantage is evident only in FPR95 for MLS and MSP, but both AUROC and FPR95 worsen for CE ( $L^2$ ).

We perform a second evaluation analysis by changing the network backbone. We experiment with a range of distinct architectures beyond the already considered DGCNN and PointNet++. Specifically, we tested CurveNet [52], GDANet [54], RSCNN [30], pointMLP [31] and PCT [18]. In particular the latter exploits Transformer blocks for point cloud learning and has recently achieved state-of-the-art performance for 3D object classification and segmentation. The results in the left part of Fig. 4 show that for various 3D backbones the Open Set performance is not strictly linked to the closed set accuracy. For low closed set accuracy values, the reference MSP method shows a linearly growing trend (CurveNet, DGCNN, PointMLP), which however disappears when considering backbones with higher closed set ACC values. For instance, RSCNN reaches one of the highest closed set accuracy results, but its AUROC is the worst one. The trend inverts for CE ( $L^2$ ), for which the high closed accuracy of RSCNN indeed corresponds to a high AUROC performance. As a side note, it is interesting to remark how PointNet++ allows getting much better results than the recent PCT.

**Are 3D Open Set approaches affected by the point cloud density?** One of the inherent characteristics of the 3D point clouds is their density. Since it clearly influences the data appearance, we expect it to affect the ability of the models to identify known and unknown samples. We propose an experimental analysis on this aspect by changing the point cloud size in 512, 1024, 2048, and 4096.

Table 3: Synthetic to Real Benchmark

| Method                | Synth to Real Benchmark - DGCNN [49] |             |             |             |             |             | Synth to Real Benchmark - PointNet++ [35] |             |             |             |             |             |
|-----------------------|--------------------------------------|-------------|-------------|-------------|-------------|-------------|---|-------------|-------------|-------------|-------------|-------------|
|                       | SR 1                                 |             | SR 2        |             | Avg         |             | SR 1                                      |             | SR 2        |             | Avg         |             |
|                       | AUROC↑                               | FPR95↓      | AUROC↑      | FPR95↓      | AUROC↑      | FPR95↓      | AUROC↑                                    | FPR95↓      | AUROC↑      | FPR95↓      | AUROC↑      | FPR95↓      |
| MSP [19]              | 72.2                                 | 91.0        | 61.2        | 90.3        | 66.7        | 90.6        | 81.0                                      | 79.6        | 70.3        | 86.7        | 75.6        | 83.2        |
| MLS [47]              | 69.0                                 | 92.2        | 62.4        | 88.9        | 65.7        | 90.5        | 82.1                                      | 76.6        | 67.6        | 86.8        | 74.8        | 81.7        |
| ODIN [28]             | 69.0                                 | 92.2        | 62.4        | 89.0        | 65.7        | 90.6        | 81.7                                      | 77.3        | 70.2        | 84.4        | 76.0        | 80.8        |
| Energy [29]           | 68.8                                 | 92.7        | 62.4        | 88.9        | 65.6        | 90.8        | 81.9                                      | 77.5        | 67.7        | 87.3        | 74.8        | 82.4        |
| GradNorm [22]         | 67.0                                 | 93.5        | 59.8        | 89.4        | 63.4        | 91.5        | 77.6                                      | 80.1        | 68.4        | 86.3        | 73.0        | 83.2        |
| ReAct [43]            | 68.4                                 | 92.1        | 62.8        | 88.8        | 65.6        | 90.5        | 81.7                                      | 75.6        | 67.6        | 87.2        | 74.6        | 81.4        |
| VAE [32]              | 68.6                                 | 77.0        | 57.9        | 92.3        | 63.3        | 84.6        | -   | -           | -           | -           | -           | -           |
| NF                    | 72.5                                 | <b>81.6</b> | <b>70.2</b> | <b>83.0</b> | 71.3        | <b>82.3</b> | 78.0                                      | 84.4        | 74.7        | 84.2        | 76.4        | 84.3        |
| OE+mixup [20]         | 71.1                                 | 89.6        | 59.5        | 92.0        | 65.3        | 90.8        | 71.2                                      | 89.7        | 60.3        | 93.5        | 65.7        | 91.6        |
| ARPL+CS [7]           | 71.5                                 | 90.2        | 62.8        | 89.5        | 67.1        | 89.8        | <b>82.8</b>                               | 74.9        | 68.0        | 89.3        | 75.4        | 82.1        |
| Cosine proto          | 58.6                                 | 90.6        | 57.3        | 91.3        | 57.9        | 91.0        | 79.9                                      | <b>74.5</b> | <b>76.5</b> | <b>77.8</b> | <b>78.2</b> | <b>76.1</b> |
| CE ( $L^2$ )          | 67.5                                 | 87.4        | 64.6        | 91.0        | 66.1        | 89.2        | 79.7                                      | 84.5        | 75.7        | 80.2        | 77.7        | 82.3        |
| SubArcFace [11]       | <b>74.5</b>                          | 86.7        | 68.7        | 86.6        | <b>71.6</b> | 86.7        | 78.7                                      | 84.3        | 75.1        | 83.4        | 76.9        | 83.8        |
| MSP (+RW Augm)        | 82.1                                 | 76.0        | 65.8        | 92.8        | 73.9        | 84.4        | 76.5                                      | 81.8        | 74.6        | 85.9        | 75.5        | 83.9        |
| SubArcFace (+RW Augm) | 81.3                                 | 77.4        | 68.8        | 84.7        | <b>75.1</b> | <b>81.1</b> | 76.9                                      | 83.7        | 73.0        | 89.5        | 75.0        | 86.6        |

For each experiment we fix the number of points (*e.g.* 512) at both training and evaluation. Higher sampling rates produce more detailed point clouds with visible fine-grained structures at the expense of increased computational complexity for the models that take them as input. The left part of Fig. 5 shows some visualizations of the influence of the sampling on the visibility of local details, which are important for both known vs unknown discrimination and closed set classification. On the right part of Fig. 5, we report the AUROC and closed set performance ACC for MSP and CE ( $L^2$ ). While the closed set accuracy grows when augmenting the number of sampled points and a similar trend is shown by the AUROC of MSP, there is not a corresponding increase for the Open Set performance of CE ( $L^2$ ) which seems agnostic to the point cloud density.

## 5 Synthetic to Real Benchmark Experiments

**Are existing 2D methods able to generalize across domains for 3D Open Set?** Tab. 3 provides an overview of the results on the Synthetic to Real Benchmark. Here the task is much more challenging with respect to the one discussed in the previous section since the models need to focus on the semantic content of the point clouds and generalize over noise, occlusion, background and all the peculiarities of the (real-world) target data not observed at training time. Indeed, with respect to Tab. 1 we notice a general degradation in performance. Interestingly, the PointNet++ backbone seems more robust to the domain shift than DGCNN. For example, on average the MSP baseline with PointNet++ outperforms the DGCNN counterpart by 8.9 points in terms of AUROC and 7.4 in terms of FPR95.

Overall, several methods that performed well in the Synthetic Benchmark turn out to be less robust than the simple MSP baseline, and no longer outperform it. This is true for the vast majority of discriminative models. The poor behaviour of VAE is similar to that already observed in the synthetic experiments. NF performs consistently on both backbones with a clear AUROC improvement of 4.6 points over MSP when applied on top of DGCNN, and only a slight improvement for PointNet++. In the case of OE+mixup, the generated outliers used to finetune the classifier model introduce some confusion with a decrease in the performance with respect to the MSP baseline (see more details in the Appendix).

The results of distance-based models are highly dependent on the specific backbone chosen. Cosine proto performs particularly well on PointNet++ but fails miserably on DGCNN. So the distribution shift amplified a behaviour that was already evident in the synthetic experiments for this method. The results of CE ( $L^2$ ) confirm the robustness of PointNet++ to the domain shift. Finally, SubArcFace demonstrates the top reliability in this setting, as it achieves good results on both backbones and the best overall results on average.

For both MSP and SubArcFace we studied the impact of several backbones also considering the closed set performance as shown in the right part of Fig. 4. The plot shows a linearly growing trend for both methods and the results also confirm the advantage of PointNet++ over more complex networks.



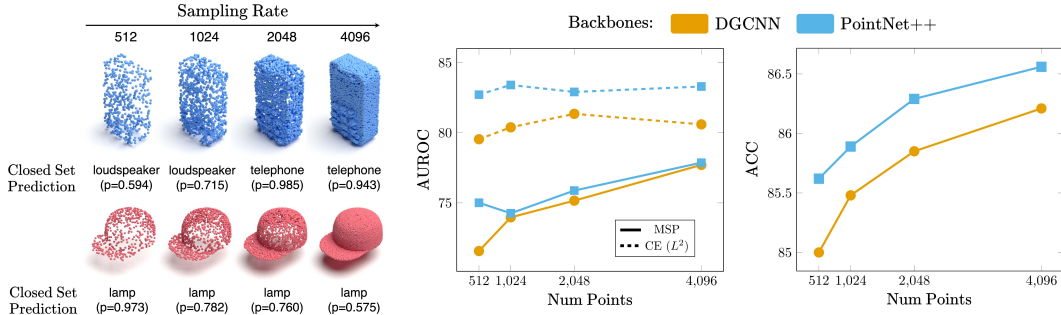


Figure 5: Analysis of the sampling rate influence on the hard SN1 set. Left: the blue-telephone and red-cap are respectively known and unknown test samples for a DGCNN classifier trained on SN1. We show the class with the highest probability (p) assignment predicted by the model trained on the closed set. With a high sampling rate the known object is correctly recognized, while for the unknown one the confidence is very low, which supports rejection. Right: AUROC and Acc trends when varying the number of sampled points.

**Does 3D Open Set across domains benefit from data augmentation?** One way to reduce the domain gap is to prepare the model for the target style by including tailored augmentations during training. Considering the nature of the real-world testing data, we adopt the *Occlusion* and *LIDAR* augmentations from [42] on the synthetic samples at training time. We perform experiments with such augmented training data for both the simple MSP baseline and SubArcFace method building on the DGCNN and PointNet++ backbones. The results are presented in the last rows of Tab. 3, where we use (+RW Augm) to refer to the models trained with the augmented training set. The DGCNN results highly benefit from the real-world tailored data augmentation, obtaining an AUROC improvement of 7.2 points and 3.5 points respectively for MSP and SubArcFace methods. This brings DGCNN up to the same level as the PointNet++ MSP baseline. On the other hand, the augmentation does not provide any further advantage to the already high PointNet++ SubArcFace results.

## 6 Conclusions

We presented the first benchmark for Open Set 3D learning that took into account several settings and two scenarios with different types of distributional shifts. Our analysis shows that cutting-edge 2D Open Set methods do not easily transfer their state-of-the-art performance to 3D data, with simple representation learning approaches like CE ( $L^2$ ) and SubArcFace often outperforming them. Moreover, the performances of the Open Set 3D methods depend on the chosen backbone: PointNet++ has shown to be highly robust across domains and provides better results than more recent and complex networks. The point density may be an issue for baseline approaches but has a minimal impact on distance-based strategies as CE ( $L^2$ ). Finally, when dealing with the combination of semantic and domain shift, Open Set on 3D data becomes extremely difficult. Basic attempts to reduce the appearance gap via data augmentation yield only marginal success on weaker backbones.

We hope that this benchmark will represent a reliable foothold for future research in this area, pushing for the development of Open Set methods tailored for 3D data and able to exploit their peculiarity.

## References

- [1] D. Abati, A. Porrello, S. Calderara, and R. Cucchiara. Latent Space Autoregression for Novelty Detection. In *CVPR*, 2019.
- [2] A. Alliegro, D. Boscaini, and T. Tommasi. Joint supervised and self-supervised learning for 3d real world challenges. In *ICPR*, 2021.
- [3] A. Bhardwaj, S. Pimpale, S. Kumar, and B. Banerjee. Empowering knowledge distillation via open set recognition for robust 3d point cloud classification. *Pattern Recognition Letters*, 151:172–179, 2021.

- [4] A. Cardace, R. Spezialetti, P. Z. Ramirez, S. Salti, and L. D. Stefano. Refrec: Pseudo-labels refinement via shape reconstruction for unsupervised 3d domain adaptation. In *3DV*, 2021.
- [5] J. Cen, P. Yun, J. Cai, M. Wang, and M. Liu. Open-set 3d object detection. In *3DV*, 2021.
- [6] A. X. Chang, T. Funkhouser, L. Guibas, P. Hanrahan, Q. Huang, Z. Li, S. Savarese, M. Savva, S. Song, H. Su, J. Xiao, L. Yi, and F. Yu. ShapeNet: An Information-Rich 3D Model Repository. *preprint arXiv:1512.03012*, 2015.
- [7] G. Chen, P. Peng, X. Wang, and Y. Tian. Adversarial reciprocal points learning for open set recognition. *IEEE Transactions on Pattern Analysis and Machine Intelligence*, 2021.
- [8] G. Chen, L. Qiao, Y. Shi, P. Peng, J. Li, T. Huang, S. Pu, and Y. Tian. Learning open set network with discriminative reciprocal points. In *ECCV*, 2020.
- [9] J. Chen, Y. Li, X. Wu, Y. Liang, and S. Jha. Atom: Robustifying out-of-distribution detection using outlier mining. In *ECML*, 2021.
- [10] S. Choi and S.-Y. Chung. Novelty detection via blurring. In *ICLR*, 2020.
- [11] J. Deng, J. Guo, T. Liu, M. Gong, and S. Zafeiriou. Sub-center arcface: Boosting face recognition by large-scale noisy web faces. In *ECCV*, 2020.
- [12] J. Deng, J. Guo, N. Xue, and S. Zafeiriou. Arcface: Additive angular margin loss for deep face recognition. In *CVPR*, 2019.
- [13] L. Dinh, J. Sohl-Dickstein, and S. Bengio. Density estimation using Real NVP. In *ICLR*, 2017.
- [14] X. Du, Z. Wang, M. Cai, and Y. Li. VOS: Learning What You Don't Know by Virtual Outlier Synthesis. In *ICLR*, 2022.
- [15] H. Fan, H. Su, and L. Guibas. A point set generation network for 3d object reconstruction from a single image. In *CVPR*, 2017.
- [16] D. Fontanel, F. Cermelli, M. Mancini, and B. Caputo. Detecting anomalies in semantic segmentation with prototypes. In *CVPR-W*, 2021.
- [17] C. Guo, G. Pleiss, Y. Sun, and K. Q. Weinberger. On calibration of modern neural networks. In *ICML*, 2017.
- [18] M.-H. Guo, J.-X. Cai, Z.-N. Liu, T.-J. Mu, R. R. Martin, and S.-M. Hu. Pct: Point cloud transformer. *Computational Visual Media*, 7(2):187–199, 2021.
- [19] D. Hendrycks and K. Gimpel. A baseline for detecting misclassified and out-of-distribution examples in neural networks. *ICLR*, 2017.
- [20] D. Hendrycks, M. Mazeika, and T. Dietterich. Deep anomaly detection with outlier exposure. In *ICLR*, 2019.
- [21] H. Huang, Z. Li, L. Wang, S. Chen, B. Dong, and X. Zhou. Feature space singularity for out-of-distribution detection. In *SafeAI-W*, 2021.
- [22] R. Huang, A. Geng, and Y. Li. On the importance of gradients for detecting distributional shifts in the wild. In *NeurIPS*, 2021.
- [23] P. Khosla, P. Teterwak, C. Wang, A. Sarna, Y. Tian, P. Isola, A. Maschinot, C. Liu, and D. Krishnan. Supervised contrastive learning. In *NeurIPS*, 2020.
- [24] S. Kong and D. Ramanan. OpenGAN: Open-Set Recognition via Open Data Generation. In *ICCV*, 2021.
- [25] D. Lee, J. Lee, J. Lee, H. Lee, M. Lee, S. Woo, and S. Lee. Regularization strategy for point cloud via rigidly mixed sample. In *CVPR*, 2021.
- [26] K. Lee, K. Lee, H. Lee, and J. Shin. A simple unified framework for detecting out-of-distribution samples and adversarial attacks. In *NeurIPS*, 2018.
- [27] Y. Li and N. Vasconcelos. Background data resampling for outlier-aware classification. In *CVPR*, 2020.
- [28] S. Liang, Y. Li, and R. Srikant. Enhancing the reliability of out-of-distribution image detection in neural networks. In *ICLR*, 2018.
- [29] W. Liu, X. Wang, J. Owens, and Y. Li. Energy-based out-of-distribution detection. In *NeurIPS*, 2020.

- [30] Y. Liu, B. Fan, S. Xiang, and C. Pan. Relation-shape convolutional neural network for point cloud analysis. In *CVPR*, 2019.
- [31] X. Ma, C. Qin, H. You, H. Ran, and Y. Fu. Rethinking network design and local geometry in point cloud: A simple residual MLP framework. In *ICLR*, 2022.
- [32] M. Masuda, R. Hachiuma, R. Fujii, H. Saito, and Y. Sekikawa. Toward unsupervised 3d point cloud anomaly detection using variational autoencoder. In *ICIP*, 2021.
- [33] L. Neal, M. Olson, X. Fern, W.-K. Wong, and F. Li. Open set learning with counterfactual images. In *ECCV*, 2018.
- [34] A. Nguyen, J. Yosinski, and J. Clune. Deep neural networks are easily fooled: High confidence predictions for unrecognizable images. In *CVPR*, 2015.
- [35] C. R. Qi, L. Yi, H. Su, and L. J. Guibas. Pointnet++: Deep hierarchical feature learning on point sets in a metric space. In *NeurIPS*, 2017.
- [36] J. Ren, P. J. Liu, E. Fertig, J. Snoek, R. Poplin, M. Depristo, J. Dillon, and B. Lakshminarayanan. Likelihood ratios for out-of-distribution detection. In *NeurIPS*, 2019.
- [37] Y. Ruan, Y. Dubois, and C. J. Maddison. Optimal representations for covariate shift. In *ICLR*, 2022.
- [38] M. Rudolph, B. Wandt, and B. Rosenhahn. Same same but different: Semi-supervised defect detection with normalizing flows. In *WACV*, 2021.
- [39] C. S. Sastry and S. Oore. Detecting out-of-distribution examples with Gram matrices. In *ICML*, 2020.
- [40] V. Schwag, M. Chiang, and P. Mittal. SSD: A Unified Framework for Self-Supervised Outlier Detection. In *ICLR*, 2021.
- [41] Y. Shu, Y. Shi, Y. Wang, T. Huang, and Y. Tian. P-ODN: Prototype-based open deep network for open set recognition. *Nature Scientific Reports*, 10(1):1–13, 2020.
- [42] J. Sun, Q. Zhang, B. Kailkhura, Z. Yu, C. Xiao, and Z. M. Mao. Benchmarking robustness of 3d point cloud recognition against common corruptions. *preprint arXiv:2201.12296*, 2022.
- [43] Y. Sun, C. Guo, and Y. Li. ReAct: Out-of-distribution Detection With Rectified Activations. In *NeurIPS*, 2021.
- [44] C. Szegedy, V. Vanhoucke, S. Ioffe, J. Shlens, and Z. Wojna. Rethinking the inception architecture for computer vision. In *CVPR*, 2016.
- [45] J. Tack, S. Mo, J. Jeong, and J. Shin. CSI: Novelty Detection via Contrastive Learning on Distributionally Shifted Instances. In *NeurIPS*, 2020.
- [46] M. A. Uy, Q.-H. Pham, B.-S. Hua, D. T. Nguyen, and S.-K. Yeung. Revisiting Point Cloud Classification: A New Benchmark Dataset and Classification Model on Real-World Data. In *ICCV*, 2019.
- [47] S. Vaze, K. Han, A. Vedaldi, and A. Zisserman. Open-Set Recognition: A Good Closed-Set Classifier is All You Need. In *ICLR*, 2022.
- [48] H. Wang, Y. Wang, Z. Zhou, X. Ji, D. Gong, J. Zhou, Z. Li, and W. Liu. Cosface: Large margin cosine loss for deep face recognition. In *CVPR*, 2018.
- [49] Y. Wang, Y. Sun, Z. Liu, S. E. Sarma, M. M. Bronstein, and J. M. Solomon. Dynamic Graph CNN for Learning on Point Clouds. *ACM Transactions on Graphics (TOG)*, 38(5):1–12, 2019.
- [50] K. Wong, S. Wang, M. Ren, M. Liang, and R. Urtasun. Identifying unknown instances for autonomous driving. In *CoRL*, 2019.
- [51] Z. Wu, S. Song, A. Khosla, F. Yu, L. Zhang, X. Tang, and J. Xiao. 3D ShapeNets: A Deep Representation for Volumetric Shapes. In *CVPR*, 2015.
- [52] T. Xiang, C. Zhang, Y. Song, J. Yu, and W. Cai. Walk in the cloud: Learning curves for point clouds shape analysis. In *ICCV*, 2021.
- [53] Z. Xiao, Q. Yan, and Y. Amit. Likelihood regret: An out-of-distribution detection score for variational auto-encoder. In *NeurIPS*, 2020.
- [54] M. Xu, J. Zhang, Z. Zhou, M. Xu, X. Qi, and Y. Qiao. Learning geometry-disentangled representation for complementary understanding of 3d object point cloud. In *AAAI*, 2021.

- [55] J. Yang, H. Wang, L. Feng, X. Yan, H. Zheng, W. Zhang, and Z. Liu. Semantically coherent out-of-distribution detection. In *ICCV*, 2021.
- [56] J. Yang, K. Zhou, Y. Li, and Z. Liu. Generalized out-of-distribution detection: A survey. *preprint arXiv:2110.11334*, 2021.
- [57] Y. Yang, C. Feng, Y. Shen, and D. Tian. FoldingNet: Point Cloud Auto-Encoder via Deep Grid Deformation. In *CVPR*, 2018.
- [58] Q. Yu and K. Aizawa. Unsupervised out-of-distribution detection by maximum classifier discrepancy. In *ICCV*, 2019.
- [59] H. Zhang, A. Li, J. Guo, and Y. Guo. Hybrid models for open set recognition. In *ECCV*, 2020.
- [60] J. Zhang, N. Inkawhich, Y. Chen, and H. Li. Fine-grained out-of-distribution detection with mixup outlier exposure. *preprint arXiv:2106.03917*, 2021.

## A Baselines details, implementation and reproducibility

We publicly release our code and data at [https://github.com/antoalli/3D\\_OS](https://github.com/antoalli/3D_OS). The repository also contains instructions on how to replicate all the experiments.

In the main paper we include a high-level description of all the considered methods and the most relevant implementation details. Here we extend the description, discussing their hyperparameters and implementation choices.

**Discriminative Methods.** All the approaches in this group (MSP, MLS, ODIN, Energy, GradNorm, ReAct) share the same basic cross-entropy classifier trained on known data. Section 3.4 of the main paper already specified the cardinality (number of points) of the point clouds in train and test, as well as the number of epochs, initial learning rate and learning rate scheduling policy.

*MSP & MLS* only differ in how the logits of the classifier on each test sample are used to compute the normality score. *MLS* directly employs the maximum logit, while for *MSP* the logits go through a softmax function before selecting the maximum of the obtained class probabilities as the score.

*ODIN* internally exploits input perturbation and temperature scaling since both affect the distribution of the softmax scores, better separating data from known and unknown classes. The most important hyperparameter here is the temperature value which we set to  $T = 1000$ , by following the original paper’s instructions [28]. The input perturbation magnitude  $\varepsilon$  should be optimized through a validation set of OOD samples, still keeping its value very small to avoid detrimental effects. Considering that we do not have access to OOD data at training time we preferred to stay on the safe side, setting  $\varepsilon = 0$  in all of our experiments, effectively disabling the input perturbation.

The *Energy* normality score is computed by postprocessing the network output logits and it’s hyperparameter free.

In order to compute the normality score for *GradNorm*, the KL divergence between the network output and a uniform distribution is backpropagated to obtain network gradients and then extract their norm. As suggested in the original paper [22], we exploit the norm of the gradients of the last layer only. No further hyperparameters are involved in this process.

*ReAct* rectifies the test-time activations of the network trained for classification and then can exploit any normality score computation strategy. By following [43] we use *ReAct* in combination with the *Energy* normality score. The only hyperparameter involved is the rectification threshold value. We chose it by exploiting the known classes validation samples to preserve 90% of ID activations. For the Synthetic Benchmark, the known classes validation samples come from the original ShapeNet-Core [6] validation split. For the Synthetic to Real Benchmark, we adopt ModelNet40 [51] known class test set as validation, we underline that these samples are not involved in the testing phase since both closed set accuracy and Open Set performance are computed on ScanObjectNN [46].

**Density and Reconstruction Based Methods.** For our *VAE* experiments we use the original code publicly released by the authors<sup>2</sup> [32], as well as their same choice on point cloud cardinality (2048 points) and hyperparameters. The encoder is composed of graph-convolutional layers: it takes as input a point cloud and outputs two 512-dimensional vectors representing the mean and variance.

<sup>2</sup>[https://github.com/lilien30/point\\_cloud\\_anomaly\\_detection](https://github.com/lilien30/point_cloud_anomaly_detection)

The decoder is a FoldingNet: it takes in input a sampled vector  $z$  from the encoded mean and variance and then outputs an intermediate and a final point cloud reconstruction with respectively 1024 and 2048 points. The normality score is computed as the Chamfer Distance [15] between the original test sample and its final reconstruction.

For the *NF* method we got inspired by [59]. The overall architecture consists of three modules: a feature encoder, a classification head, and a normalizing flow head. The feature encoder and classification head work together to optimize a standard cross-entropy loss. The normalizing flow head works independently on top of the feature encoder representation and it is composed of eight Real-NVP [13] coupling blocks which are trained to maximize the log-likelihood of the observed training features. At inference time we use the test sample log-likelihood as a normality score. For training *NF* we use the Adam optimizer with a learning rate of 0.0002 and weight decay set to 0.00001.

**Outlier Exposure with OOD Generated Data.** The outlier exposure strategy described in [20] consists in training a Discriminative Model on ID training data (known) through standard cross-entropy loss, while exploiting additional OOD training data (unknown) to improve ID-OOD separability. Specifically, we start from the same cross-entropy classifier trained on known classes employed for the first group of strategies (*i.e.* Discriminative Models) and finetune it by minimizing the following loss function:  $\mathcal{L}_{ft} = \mathcal{L}_{CE,known} + \lambda \mathcal{L}_{OE,unknown}$ .

The finetuning involves a continued optimization of the cross-entropy loss on known training data  $\mathcal{L}_{CE,known}$  and an outlier exposure objective  $\mathcal{L}_{OE,unknown}$  on unknown training data. The goal of the outlier exposure objective is to minimize the KL divergence between the Uniform and Cross-entropy distributions for unknown samples. The hyperparameter  $\lambda$  controls the importance of the OE auxiliary objective and is set to 0.5 according to the original paper [20]. The finetuning is performed for additional 100 epochs, with a learning rate reduced by a factor of 100.

For OE finetuning, OOD training data are obtained through Rigid Subset Mix (RSMix) [25] of known classes samples. Fig. 6 shows some examples of the produced OOD data for the synthetic SN1 set.

**Representation and Distance Based Methods.** The *ARPL+CS* method entails training a GAN model to generate confusing samples (CS) and optimizing the reciprocal points learning objective. To keep all of the learning components balanced, this method relies on several hyperparameters. In our experiments we used the same hyperparameters adopted by the authors [7].

For *Cosine proto* we train a simple cosine classifier by following the CosFace [48] strategy and setting the imposed margin to 0. At inference time, the output logits correspond to the cosine similarities between the test sample and the class prototypes. The largest value is used as a normality score without introducing additional hyperparameters.

The goal of *CE* ( $L^2$ ) is to investigate the dependability of a classifier’s feature representation for OOD detection. We use the inverse of the distance from the nearest training sample as each test sample normality score, without introducing any additional hyperparameters.

*SupCon* requires a long training with a large batch size to reach convergence [23]. With respect to the models trained for classification we double the batch size and halve the learning rate. To deal with large batches we perform distributed training on multiple GPUs and adopt Synchronized Batch Normalization. We also increase the number of epochs to 2000, using a linear warm-up in the first 100. During inference, the normality score is the cosine similarity of each test sample to its nearest training sample. The *SupCon* learning objective builds a hyperspherical feature space in which class clusters are compact and well separated. Similar results can be obtained through *SubArcFace* which exploits a much more easily optimized classification loss. On this basis, and also considering the poor results of *SupCon* on the Synthetic Benchmark, we decided to discard it in the Synthetic to Real Benchmark.

The learning objective of *SubArcFace* seeks to maximize the cosine similarity between each training sample and one of the  $K$  centers associated with its respective class, while also imposing a certain margin  $m$  between different classes. We use  $K = 3$  as done by the authors in the original paper [11] and set the margin to  $m = 0.5$ , as done in *ArcFace* [12] from which this hyperparameter is inherited. The normality score is computed as done for *SupCon*.

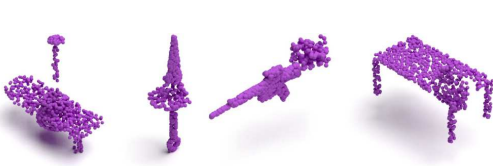


Figure 6: Examples of RSMix [25] between known samples of the synthetic SN1 set. We employ these mixed point clouds as training OOD data in OE experiments.



Figure 7: Examples of ModelNet point clouds augmented with LIDAR (first two) and Occlusion (last two) corruptions from [42].

Table 4: Synthetic to Real Benchmark with data augmentation

| Synth to Real Benchmark - DGCNN [49] |             |             |             |             |             | Synth to Real Benchmark - PointNet++ [35] |             |             |             |             |             |             |
|--------------------------------------|-------------|-------------|-------------|-------------|-------------|---|-------------|-------------|-------------|-------------|-------------|-------------|
| Method                               | SR 1        |             | SR 2        |             | Avg         |   | SR 1        |             | SR 2        |             | Avg         |             |
|                                      | AUROC↑      | FPR95↓      | AUROC↑      | FPR95↓      | AUROC↑      | FPR95↓                                    | AUROC↑      | FPR95↓      | AUROC↑      | FPR95↓      | AUROC↑      | FPR95↓      |
| MSP [19]                             | 72.2        | 91.0        | 61.2        | 90.3        | 66.7        | 90.6                                      | 81.0        | 79.6        | 70.3        | 86.7        | 75.6        | 83.2        |
| MLS [47]                             | 69.0        | 92.2        | 62.4        | 88.9        | 65.7        | 90.5                                      | <b>82.1</b> | <b>76.6</b> | 67.6        | 86.8        | 74.8        | <b>81.7</b> |
| SubArcFace [11]                      | <b>74.5</b> | 86.7        | 68.7        | 86.6        | <b>71.6</b> | 86.7                                      | 78.7        | 84.3        | <b>75.1</b> | <b>83.4</b> | <b>76.9</b> | 83.8        |
| MSP (+LIDAR)                         | 74.4        | 85.5        | 62.5        | 90.3        | 68.5        | 87.9                                      | 76.3        | 83.7        | 72.6        | 87.7        | 74.5        | 85.7        |
| MSP (+Occlusion)                     | 81.3        | 77.4        | 63.2        | 93.7        | 72.2        | 85.5                                      | 73.2        | <b>81.1</b> | <b>75.3</b> | <b>84.9</b> | 74.3        | <b>83.0</b> |
| MSP (+RW Augm)                       | 82.1        | 76.0        | 65.8        | 92.8        | 73.9        | 84.4                                      | 76.5        | 81.8        | 74.6        | 85.9        | 75.5        | 83.9        |
| SubArcFace (+LIDAR)                  | 77.0        | 85.5        | 63.6        | 85.7        | 70.3        | 85.6                                      | <b>78.2</b> | 85.9        | 73.6        | 87.9        | <b>75.9</b> | 86.9        |
| SubArcFace (+Occlusion)              | 82.1        | <b>73.8</b> | 39.7        | 96.7        | 60.9        | 85.2                                      | 77.8        | <b>81.1</b> | 73.5        | 86.4        | 75.7        | 83.7        |
| SubArcFace (+RW Augm)                | 81.3        | 77.4        | <b>68.8</b> | <b>84.7</b> | <b>75.1</b> | <b>81.1</b>                               | 76.9        | 83.7        | 73.0        | 89.5        | 75.0        | 86.6        |

## B Synthetic to Real Experiments

The goal of the Synthetic to Real Benchmark is to simulate realistic deployment conditions and analyze the behaviour of Open Set methods in this context. Due to the high cost of 3D data acquisition and labelling, large synthetic datasets are commonly used to train deep neural network models which are then employed in real-world applications such as autonomous driving, augmented reality or robotics. This strategy, although effective in lowering data collection costs, inevitably causes a distribution shift between training and test data. Note that the test samples cover both the known training classes and the novel unknown ones, so we experience both a semantic and a domain shift.

As shown by Fig. 1 of the main paper, real-world samples (in yellow) are much noisier than synthetic ones (in blue). Moreover, real-world point clouds have background (first chair), are affected by occlusion (second chair) and interaction with other objects nearby (second sofa, first chair).

Fig. 6 presents point cloud instances obtained via mixup. This strategy is used to create data that can be exploited as OOD during training via outlier exposure. However, as it can be noticed, shape mixing inevitably introduces some artefacts that resemble noise and background, typical of real-world data. We believe that in the synthetic-to-real experiments this may introduce some confusion rather than helping in separating known and unknown classes, as it pushes the model to believe that all corrupted samples belong to unknown classes. This reflects in the poor *OE+mixup* results reported in Tab. 3 of the main paper.

Finally, in the last paragraph of Sec. 5 of the main paper we discussed the possibility to improve the performance on the Synthetic to Real Benchmark by exploiting additional data augmentations. In particular, we analyzed two types of transformations called LIDAR and Occlusion which were presented in [42] and that allowed us to obtain a performance improvement mainly with the DGCNN backbone. The objective of this augmentation strategy is in fact to emulate on training samples some of the corruptions that appear in real-world data. In Fig. 7 we show some augmented training samples. In Tab. 4, we also show the individual results obtained with each augmentation, in addition to the combined results (+RW Augm). For what concerns the experiments with the DGCNN [49] backbone, we can see that both augmentations already improve the MSP results individually, providing an even greater improvement when they are applied together. With SubArcFace the individual augmentations oddly cause damage to the performance, at least in terms of AUROC. Nonetheless, combining them results in an improvement, most likely due to the higher data variability. The behavior with PointNet++ [35] is the same in the case of individual or combined augmentations: the

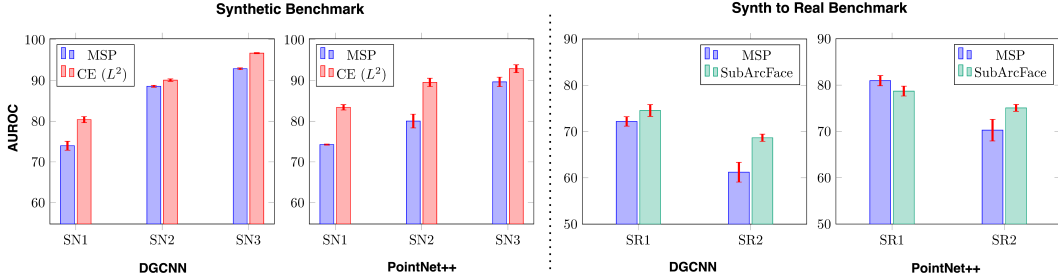


Figure 8: Error margin analysis. State-of-the-art and baseline AUROC results on the three Synthetic Benchmark cases and the two Synthetic to Real cases. Red error bars represent the standard deviation around the mean value.

already high results that this backbone obtains in the Synthetic to Real Benchmark do not leave room for improvements with tailored augmentation protocols.

## C Analysis of the error margin

All the experimental results presented in the main paper are average over three experiments repetitions with different seeds. In Fig. 8 we report both average and standard deviation for the methods that presented top results, respectively CE ( $L^2$ ) for the *Synthetic* and SubArcFace for the *Synthetic to Real* Benchmarks, together with the MSP baseline. By looking at the error bars, we can see that in the Synthetic Benchmark the standard deviation is quite small and the advantage of CE ( $L^2$ ) over MSP is always statistically significant. In the Synthetic to Real Benchmark the performance gap is lower, especially for the SR1 case, where MSP outperforms SubArcFace with the PointNet++ backbone. However, with both backbones the results of the baseline and the state-of-the-art approach are within the error margin. On the other hand, SubArcface has significantly better performance on the SR2 setting with also a smaller standard deviation.

## D Limitations

Some limitations of our work are directly inherited from the 3D computer vision field. The benchmark would certainly benefit from the inclusion of a large-scale real-world dataset: unfortunately, such a dataset should be collected and curated on purpose since it is currently unavailable. In the last year, huge progress has been made in 3D deep learning literature, however most of the recent works exclusively focus on synthetic scenarios, now exhibiting a trend of performance saturation on these testbeds. Furthermore, the lack of a large-scale annotated dataset also limits the development of more efficient 3D backbones. With our experiments, we have shown that employing a cutting-edge backbone does not automatically translate into better performance. This surprising trend is even more visible in the synthetic to real-world scenario, for which more research efforts are needed. For what concerns the distance-based methods that have shown the best results in our analysis (CE ( $L^2$ ), SubArcFace), it is important to highlight that they need the whole training set available at test time. Indeed, the prediction depends on the distance of the test sample to the closest training instance. The deployment of Open Set discriminative methods, on the other hand, is less demanding because it involves using a closed-set trained model, despite their lower performance. Overall it would be desirable an Open Set model that combines the best of both worlds (fast deployment and high results).

## E Broader Impact

We hope that our research will have a positive impact on both academia and society. In terms of academic research, we emphasized the importance of investigating Open Set scenarios for 3D deep learning. In this context, our benchmark will serve as a reliable starting point for novel methods capable of leveraging the plethora of information naturally offered by 3D data. We release our code with the aim of providing a foothold for future work toward building trustworthy systems that can manage the challenges of the open world. In terms of societal impact, we anticipate that increased

academic interest in this field will drive the development of more robust models for safety-critical applications where 3D sensing could be a valuable ally: autonomous driving, robotics and health care are only some examples.